

# The Origin and Control of the Sources of Anisotropic Magnetoresistance in (Ga,Mn)As Devices

A. W. Rushforth,<sup>1</sup> K. Výborný,<sup>2</sup> C. S. King,<sup>1</sup> K. W. Edmonds,<sup>1</sup> R. P. Campion,<sup>1</sup> C. T. Foxon,<sup>1</sup> J. Wunderlich,<sup>3</sup> A. C. Irvine,<sup>4</sup> P. Vašek,<sup>2</sup> V. Novák,<sup>2</sup> K. Olejník,<sup>2</sup> T. Jungwirth,<sup>2,1</sup> and B. L. Gallagher<sup>1</sup>

<sup>1</sup>*School of Physics and Astronomy, University of Nottingham, Nottingham NG7 2RD, UK*

<sup>2</sup>*Institute of Physics ASCR, Cukrovarnická 10, 162 53 Praha 6, Czech Republic*

<sup>3</sup>*Hitachi Cambridge Laboratory, Cambridge CB3 0HE, UK*

<sup>4</sup>*Microelectronics Research Centre, Cavendish Laboratory, University of Cambridge, CB3 0HE, UK*

(Dated: February 8, 2020)

(Ga,Mn)As ferromagnetic semiconductors with tuneable, strongly spin-orbit coupled and exchange split Fermi surfaces of carriers are particularly favourable systems for exploring the extraordinary magnetoresistance effects. In this experimental and theoretical study we show how the non-crystalline and crystalline sources of the anisotropic magnetoresistance (AMR) emerge in these ferromagnets, and how their relative strengths can be controlled by the device and material parameters. Measurements on standard Hall bars orientated along different crystallographic axes allow the separation of the leading non-crystalline AMR term, and the crystalline components, while in Corbino disk devices the AMR is dominated by cubic and uniaxial crystalline terms. In an ultra-thin (Ga,Mn)As material we report a realization of a unique ferromagnetic system whose large AMR response is dominated by the uniaxial crystalline term. We also demonstrate local control of the AMR by lithographically inducing lattice relaxation in microscopic Hall bars.

PACS numbers: 75.47.-m, 75.50.Pp, 75.70.Ak

Magnetoresistance (MR) effects comprise the ordinary responses of carriers to the Lorentz force produced by the external magnetic field and the extraordinary responses to internal magnetization in ferromagnets via spin-orbit interaction. Advanced computational techniques and experiments in new unconventional ferromagnets have recently led to a significant progress in coping with the subtle, relativistic nature of the extraordinary effects. There are two distinct extraordinary MR coefficients, the anomalous Hall effect and the anisotropic magnetoresistance (AMR). The former coefficient has, so far, attracted more interest and (Ga,Mn)As has become one of the favourable test bed systems for its investigation [1]. Here the unique position of (Ga,Mn)As ferromagnets stems from their tuneability and the relatively simple, yet strongly spin-orbit coupled and exchange split carrier Fermi surfaces [2, 3].

Despite its historical importance in magnetic recording technologies the understanding of the AMR effect is relatively poor [4]. Phenomenologically, AMR has non-crystalline components, arising from the lowering of the symmetry by imposing a specific current direction, and crystalline components arising from the underlying crystal symmetries of the material [5, 6, 7]. In conventional metal ferromagnets a physically appealing picture has been used to interpret the non-crystalline AMR. In the model a perturbing spin-orbit potential mixes the exchange-split spin-up and spin-down  $d$ -states in a way which leads to an anisotropic  $s - d$  scattering of the unpolarized  $s$ -like carriers [4, 8]. However, this picture has only a limited predictive power and the complicated band-structure of the conventional ferromagnets makes it

notoriously difficult to marry the basic model arguments with accurate numerical results of microscopic transport theories [9].

In this Letter we exploit the favourable characteristics of (Ga,Mn)As for exploring the AMR [7, 10, 11]. We cast new light on the old problem of the origins of the effect by explaining how the non-crystalline and crystalline sources of the AMR emerge in this material. Measurements on standard Hall bars orientated along different crystallographic axes are then used to separate the non-crystalline and crystalline components. We show that the crystalline terms can be directly measured in Corbino devices in which the cylindrical symmetry results in an averaging over all current directions in the plane of the film, eliminating the non-crystalline AMR components. In thicker, more metallic (Ga,Mn)As layers the non-crystalline term dominates, but in ultra-thin (Ga,Mn)As layers we find that the AMR is highly unconventional, showing a large AMR dominated by a uniaxial crystalline component. Finally we present measurements in microscopic,  $1\mu\text{m}$  wide Hall bars, in which an additional uniaxial term is introduced by lithography inducing local lattice relaxations [12].

Experimental data presented in this paper were measured in  $25\text{nm}$  and  $5\text{nm}$   $\text{Ga}_{0.95}\text{Mn}_{0.05}\text{As}$  films grown by low temperature molecular beam epitaxy under a compressive strain on a GaAs [001] substrate. Optical lithography was used to fabricate standard Hall bars of width  $45\mu\text{m}$  with voltage probes separated by  $285\mu\text{m}$  along the [100], [010], [110] and [ $\bar{1}\bar{1}0$ ] directions, and Corbino disks of inner diameter  $800\mu\text{m}$  and outer diameter  $1400\mu\text{m}$ . In addition, electron beam lithography was used to fabricate

1  $\mu\text{m}$  wide Hall bars in a 25 nm  $\text{Ga}_{0.95}\text{Mn}_{0.05}\text{As}$  film. Longitudinal MR in the Corbino disk and longitudinal and transverse MRs in the Hall bars were measured with the magnetization in the plane of the device, i.e., in the pure AMR geometry with zero (antisymmetric) Hall signal.

We start our discussion with general considerations regarding AMR in the p-type (Ga,Mn)As diluted magnetic semiconductors. The conclusions are based on theoretical analysis and measurements in the above films complemented by experiments in a set of additional as-grown and annealed epilayers of variable nominal Mn concentrations. Extending the standard phenomenological analysis, first introduced by Döring for cubic Ni [5], to systems with cubic [100] plus uniaxial [110] anisotropy, we can write the longitudinal AMR as

$$\frac{\Delta\rho_{xx}}{\rho_{av}} = C_I \cos 2\phi + C_U \cos 2\psi + C_C \cos 4\psi + C_{I,C} \cos(4\psi - 2\phi). \quad (1)$$

Here  $\Delta\rho_{xx} = \rho_{xx} - \rho_{av}$ ,  $\rho_{av}$  is the measured  $\rho_{xx}$  averaged over  $360^\circ$  in the plane of the film,  $\phi$  is the angle between magnetization and current, and  $\psi$  the angle between magnetization and the [110] crystal direction. The four contributions are the non-crystalline term, the lowest order uniaxial and cubic crystalline terms, and a crossed non-crystalline/crystalline term. We have omitted the higher order terms in Eq. (1) as these are found to be negligibly small in our devices. The purely crystalline terms are excluded by symmetry for  $\rho_{xy}$  and we obtain

$$\frac{\Delta\rho_{xy}}{\rho_{av}} = C_I \sin 2\phi - C_{I,C} \sin(4\psi - 2\phi). \quad (2)$$

Our arguments explaining the emergence of the individual AMR sources in (Ga,Mn)As are based on microscopic theory calculations combining the six-band  $\mathbf{k} \cdot \mathbf{p}$  description of the GaAs host valence band with kinetic-exchange model of the coupling to the local  $\text{Mn}_{\text{Ga}}$   $d^5$ -moments [13]. The theory is well suited for the description of spin-orbit coupling phenomena near the top of the valence band whose spectral composition and related symmetries are dominated, as in the familiar GaAs host, by the  $p$ -orbitals of the As sublattice [14]. Figures 1(a) and (b) illustrate the anisotropy of carrier scattering rates off Mn acceptors [11] on a color-coded minority heavy-hole Fermi surface for uncompensated (one hole per Mn)  $\text{Ga}_{0.95}\text{Mn}_{0.05}\text{As}$ . Here red color corresponds to strong scattering and blue color to weak scattering. The effect follows from the generic symmetry of the hole Hamiltonian and is highlighted by first considering a spherical approximation form of the Hamiltonian,  $(\hbar^2/2m)[k^2(\gamma_1 + 5/2\gamma_2) - 18\gamma_2(\mathbf{k} \cdot \mathbf{s})^2] + h\hat{\mathbf{M}} \cdot \mathbf{s}$ , where  $h$  is the exchange field,  $\hat{\mathbf{M}}$  is the magnetization unit vector,  $\mathbf{s}$  is the hole spin, and  $\gamma_{1,2}$  are material constants specific for a particular III-V host [3]. As shown in the

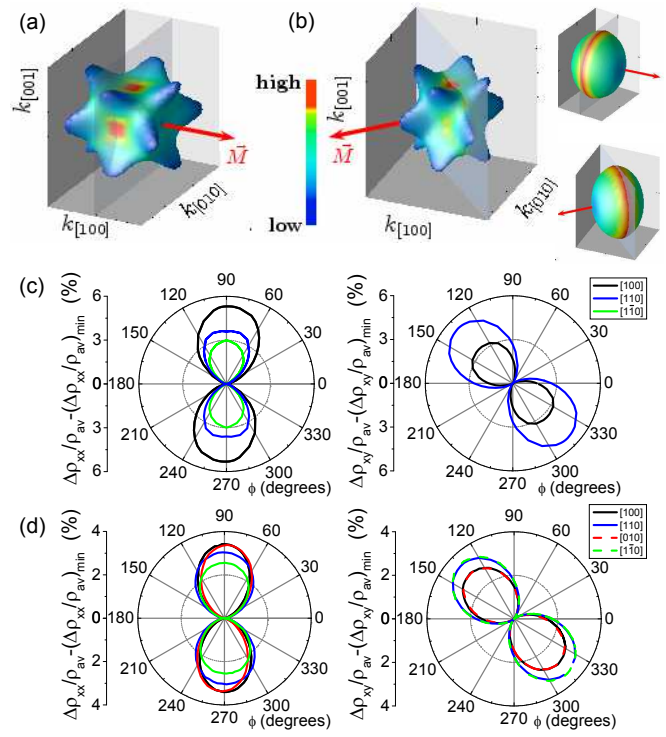


FIG. 1: (a)-(b) The calculated anisotropy of the scattering rate off Mn acceptors at the Fermi surface of the minority heavy-hole band in  $\text{Ga}_{0.95}\text{Mn}_{0.05}\text{As}$  for different magnetization directions. The colour represents the scattering rate. The insets represent the same calculations for the spherical approximation Hamiltonian (see text). (c) Calculated and (d) measured (at 4.2 K) longitudinal and transverse AMR for  $\text{Ga}_{0.95}\text{Mn}_{0.05}\text{As}$  as a function of the angle between magnetization in the plane of the film and the current. The legend shows the direction of the current. The y-axes show  $\Delta\rho/\rho_{av}$  shifted such that the minimum is at zero, to show the symmetries present in the data more clearly.

insets of Figs.1(a),(b), the strong quasiparticle scattering occurs around  $\mathbf{k} \perp \hat{\mathbf{M}}$  wavevectors, i.e., around the degeneracy line of the majority and minority hole bands of the above approximate Hamiltonian. The main panels in Figs.1(a),(b) show a clear signature, albeit more complex in structure, of the enhanced scattering of quasiparticles moving perpendicular to  $\hat{\mathbf{M}}$  in the more realistic six-band Hamiltonian. This anisotropy in the scattering rate is the source of the non-crystalline component of the AMR. The more subtle dependence of the overall topography of the anisotropic Fermi surface and the corresponding average scattering rate on the orientation of magnetization generates the crystalline AMR terms. They are the transport analogs of the magneto-crystalline anisotropy and, for in-plane magnetizations, reflect the biaxial cubic anisotropy of these zincblende compounds combined with a [110] uniaxial component. (The microscopic origin of the uniaxial symmetry breaking mechanism in the (Ga,Mn)As epilayers is not known but is modelled by a

weak in-plane shear strain [15].)

A detailed theoretical analysis of relaxation rate anisotropies in (Ga,Mn)As ferromagnets will be given elsewhere. Here we conclude the theory discussion by showing in Fig.1(c) Boltzman equation calculations [11] of the AMR for the  $\text{Ga}_{0.95}\text{Mn}_{0.05}\text{As}$  material. The non-crystalline AMR source contributes strongly and, as explained in the above paragraph, leads to a higher resistance state for  $\mathbf{I} \perp \mathbf{M}$ . Differences among AMRs for current along the [100], [110], and [1 $\bar{1}$ 0] directions show that cubic and uniaxial crystalline terms are also sizable. This phenomenology is systematically observed in experimental AMRs of weakly or moderately compensated metallic (Ga,Mn)As films. Typical data for such systems, represented by the 25nm  $\text{Ga}_{0.95}\text{Mn}_{0.05}\text{As}$  film with 3.6% AMR, are shown in Fig.1(d) for the Hall bars patterned along the [100], [010], [110], and [1 $\bar{1}$ 0] directions. In these measurements a saturating magnetic field of 1T is applied in the plane of the film and the magnetization vector follows the external field direction. Note that the leading role of the non-crystalline term is reminiscent of AMR data in most conventional transition metal ferromagnets [4, 8]. The sign, however, is opposite in these two classes of itinerant ferromagnets, reflecting the distinct orbital characters of the carriers.

A direct measurement of the crystalline components of the AMR can be made using the Corbino geometry. Here, averaging over the radial current lines eliminates all effects originating from a specific direction of the current. Measured results for a Corbino device fabricated from the same 25nm  $\text{Ga}_{0.95}\text{Mn}_{0.05}\text{As}$  film as used for the Hall bars are shown in Fig. 2(a). The AMR signal is an order of magnitude weaker than in the Hall bars and is clearly composed of a uniaxial and a cubic contribution. Figure 2(a) also shows the crystalline components of the AMR extracted from the data from the Hall Bars, by using Eqs. (1) and (2) and different combinations of the data [16]. The close agreement between the data from the two types of device confirms the validity of our phenomenological analysis. Figure 2(b) shows the coefficients  $C_{I,C}$ ,  $C_U$  and  $C_C$  extracted from the Hall bars and Corbino data over the whole range up to the Curie temperature (80K). The uniaxial crystalline term,  $C_U$  becomes the dominant term for  $T \geq 30\text{K}$ . This correlates with the uniaxial component of the magnetic anisotropy becoming dominant for  $T \geq 30\text{K}$  as observed by SQUID magnetometry measurements (not shown). Our work shows that in (Ga,Mn)As ferromagnets, the symmetry breaking mechanism behind the previously reported [15] uniaxial magneto-crystalline anisotropy in the magnetization also contributes to the magnetotransport.

We now discuss measurements on Hall bars and Corbino disk devices fabricated from ultra thin 5nm  $\text{Ga}_{0.95}\text{Mn}_{0.05}\text{As}$  films [17]. Measurements on the Hall bars in Fig. 3(a) show that the AMR is very different from that observed in the 25nm film. Application

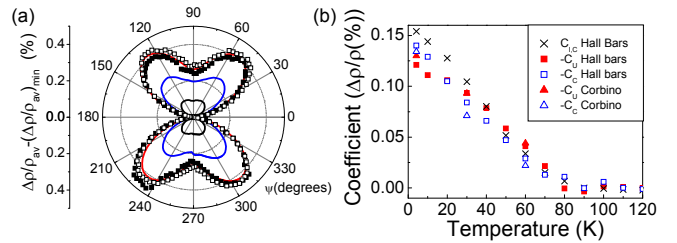


FIG. 2: (a) AMR of the 25nm  $\text{Ga}_{0.95}\text{Mn}_{0.05}\text{As}$  film in the Corbino geometry at 4.2 K (red line), 30 K (blue line), and 60 K (black line) and the crystalline component extracted from the Hall bars  $(\text{AMR}[110]+\text{AMR}[1\bar{1}0])/2$  (closed points) and  $(\text{AMR}[100]+\text{AMR}[010])/2$  (open points). (b) Temperature dependence of the crystalline terms extracted from the Hall bars and Corbino devices.

of the phenomenological analysis to the Hall bar data shows that this behaviour is a consequence of the crystalline sources dominating the AMR with the uniaxial crystalline term being the largest. SQUID magnetometry on 5nm  $\text{Ga}_{0.95}\text{Mn}_{0.05}\text{As}$  films consistently shows that the uniaxial component of the magnetic anisotropy dominates over the whole temperature range [18]. The Corbino disk AMR data, shown in Fig. 3(b) confirm our observation of the highly unconventional magnetoresistance response in which a 6% AMR is totally dominated by the uniaxial crystalline term.

The 5nm films have lower Curie temperatures ( $T_C \approx 30\text{K}$ ) than the 25nm films and become highly resistive at low temperature indicating that they are close to a metal-insulator transition. In contrast, the 25nm films show metallic behaviour at low temperatures. This indicates that the 5nm films are significantly more compensated than the 25nm films. A suppressed role of the non-crystalline AMR and an enhancement of the crystalline AMR terms in more compensated and more resistive (Ga,Mn)As epilayers is a trend consistent with our theoretical calculations and is observed in thicker films with variable Mn dopings or post-growth annealing treatments. Nevertheless, the strength of the effect in the 5 nm films is remarkable. This might be related to the expectation that the magnetic interactions become more anisotropic with increasing localization of the holes near their parent Mn ions [3].

Finally, we demonstrate how the crystalline components can be tuned by the use of lithographic patterning to induce an additional uniaxial anisotropy in very narrow Hall bars. In recent studies [12] it has been found that the lithographic patterning allows the in-plane compressive strain in the (Ga,Mn)As film to relax in the direction along the width of the Hall bar and this can lead to an additional uniaxial component in the magnetic anisotropy for bars with widths on the order of  $1\mu\text{m}$  or smaller. Figures 3(c) and (d) show the AMR of macroscopic  $45\mu\text{m}$  wide bars and  $1\mu\text{m}$  wide bars fab-

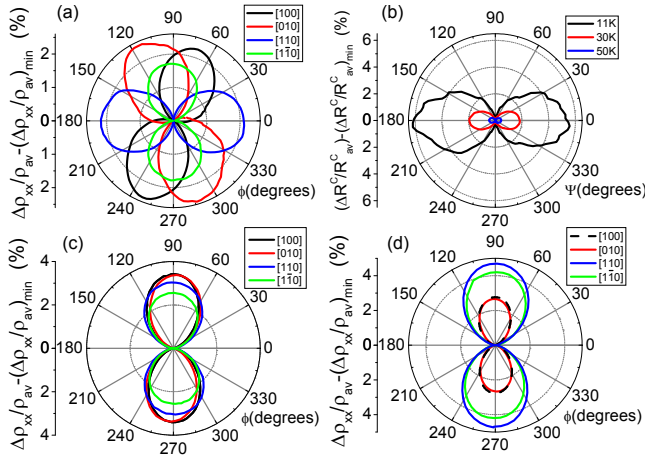


FIG. 3: Longitudinal AMR of the 5nm  $\text{Ga}_{0.95}\text{Mn}_{0.05}\text{As}$  Hall bars.  $T=20\text{K}$ . (b) AMR of a 5nm  $\text{Ga}_{0.95}\text{Mn}_{0.05}\text{As}$  film in the Corbino geometry. (c) AMR for macroscopic Hall bars and (d) narrow ( $1\mu\text{m}$  wide) Hall bars.

riated from 25nm  $\text{Ga}_{0.95}\text{Mn}_{0.05}\text{As}$  wafers [19]. For the macroscopic bars, the cubic crystalline symmetry leads to the AMR along [100] and [010] being larger than along [110] and [110]. For the narrow bars we observe the opposite relationship. This is consistent with the addition of an extra uniaxial component to the AMR which adds 0.8% to the AMR when current is along [110] and [110] and subtracts 0.4% when the current is along [100] and [010]. These are significant fractions of the total AMR. The difference in magnitude in this additional term may reflect differences in the strain relaxation along different crystallographic axes.

In summary we have demonstrated that  $(\text{Ga},\text{Mn})\text{As}$  is an ideal itinerant ferromagnet system for a systematic experimental exploration and theoretical elucidation of the origins of the AMR. Our combined measurements in Hall bar and Corbino geometries were used to unambiguously extract the distinct, non-crystalline and crystalline sources of the AMR. We have reported unique phenomenology including a large AMR completely dominated by the uniaxial crystalline term and the control of the AMR response by means of local lattice relaxations induced in lithographically patterned narrow Hall bars.

We acknowledge collaborations with J. Chauhan, D. Taylor, K.Y. Wang, M. Cukr, and M. Sawicki, and support from EU Grant IST-015728, from UK Grant GR/S81407/01, from CR Grants 202/05/0575, 202/04/1519, FON/06/E002, AV0Z1010052, and LC510.

*High Magnetic Fields*, edited by I. Vagner (Kluwer, Dordrecht, 2003), p. 197, cond-mat/0306484.

- [2] F. Matsukura, H. Ohno, and T. Dietl, in *Handbook of Magnetic Materials*, edited by K. H. J. Buschow (Elsevier, Amsterdam, 2002), 14, p. 1.
- [3] T. Jungwirth, J. Sinova, J. Mašek, J. Kučera, and A. H. MacDonald, Rev. Mod. Phys. **78**, 809 (2006).
- [4] T. McGuire and R. Potter, IEEE Trans. Magn. **11**, 1018 (1975).
- [5] W. Döring, Ann. Phys. (Leipzig) **32**, 259 (1938).
- [6] R. P. van Gorkom, J. Caro, T. M. Klapwijk, and S. Radelaar, Phys. Rev. B **63**, 134432 (2001) and references therein.
- [7] W. Limmer, M. Glunk, J. Daeubler, T. Hummel, W. Schoch, R. Sauer, C. Bihler, H. Huebl, M. S. Brandt and S. T. B. Goennenwein, Phys. Rev. B **74**, 205205 (2006); K. Y. Wang, K. W. Edmonds, R. P. Campion, L. X. Zhao, C. T. Foxon, and B. L. Gallagher, Phys. Rev. B **72**, 085201 (2005).
- [8] J. Smit, Physica **XVI**, 612 (1951); O. Jaoul, I. A. Campbell and A. Fert, J. Mag. Mag. Mat. **5**, 23 (1977).
- [9] J. Banhart and H. Ebert, Europhys. Lett. **32**, 517 (1995); H. Ebert, A. Vernes, and J. Banhart, Solid State Commun. **113**, 103 (2000); S. Khmelevskyi, K. Palotás, L. Szunyogh, and P. Weinberger, Phys. Rev. B **68**, 012402 (2003).
- [10] D. V. Baxter, D. Ruzmetov, J. Scherschligt, Y. Sasaki, X. Liu, J. K. Furdyna, and C. H. Mielke, Phys. Rev. B **65**, 212407 (2002); H. X. Tang, R. K. Kawakami, D. D. Awschalom, and M. L. Roukes, Phys. Rev. Lett. **90**, 107201 (2003).
- [11] T. Jungwirth, J. Sinova, K. Y. Wang, K. W. Edmonds, R. P. Campion, B. L. Gallagher, C. T. Foxon, Q. Niu, and A. H. MacDonald, Appl. Phys. Lett. **83**, 320 (2003).
- [12] J. Wenisch, C. Gould, L. Ebel, *et al.*, to be published, cond-mat/0701479; J. Wunderlich, T. Jungwirth, A. C. Irvine, *et al.*, to be published.
- [13] T. Dietl, H. Ohno, and F. Matsukura, Phys. Rev. B **63**, 195205 (2001); M. Abolfath, T. Jungwirth, J. Brum, and A. H. MacDonald, Phys. Rev. B **63**, 054418 (2001).
- [14] Previous applications of the theory have explained, e.g., the observed transitions between in-plane and out-of-plane easy magnetization orientations in  $(\text{Ga},\text{Mn})\text{As}$  epilayers grown under compressive and tensile strains and provided a consistent account of the signs and magnitudes of corresponding AMR effects [3].
- [15] M. Sawicki, K-Y. Wang, K. W. Edmonds, R. P. Campion, C. R. Staddon, N. R. S. Farley, C. T. Foxon, E. Papis, E. Kamińska, A. Piotrowska, T. Dietl, and B. L. Gallagher, Phys. Rev. B **71**, 121302(R) (2005).
- [16] Strictly, in a Corbino geometry we measure  $G^C = I/V = (\sigma_{xx} + \sigma_{yy})/2$  and plot  $R^C = 1/G^C$ . If we define  $R^C = 1/G^C$  and note that  $\rho_{xy} \ll \rho_{xx}$  then it is possible to show that  $\Delta R^C/R_{av}^C \approx (\Delta R_{[110]} + \Delta R_{[1\bar{1}0]})/R_{av}$  from the Hall bars =  $C_U \cos 2\psi + C_C \cos 4\psi$ .
- [17] Two wafers were used for the different devices. These had the same growth conditions and similar magnetic properties measured by SQUID magnetometry.
- [18] A. W. Rushforth, A. D. Giddings, K. W. Edmonds, R. P. Campion, C. T. Foxon, B. L. Gallagher, Phys. Stat. Sol. (c) **3**, 4078-4081 (2006).
- [19] Two different wafers with the same growth parameters were used for these devices. The intrinsic crystalline terms were found to be comparable for each wafer.